PAPER NO.

1566

REVERSED BENDING FATIGUE TESTS OF AISI 347 STAINLESS STEEL FIBERMETAL

by

Carl E. Rucker

NASA Langley Research Center
Langley Station, Hampton, Va.

Presented at

1969 SESA FALL MEETING

HOUSTON, TEXAS

OCTOBER 14-17

SOCIETY FOR
EXPERIMENTAL STRESS ANALYSIS
21 BRIDGE SQUARE WESTPORT, CONNECTICUT

REVERSED BENDING FATIGUE TESTS OF AISI 347 STAINLESS STEEL FIBERMETAL

The effects of varying density, thickness, wire diameter and stiffness parameters of candidate materials for acoustic treatment of aircraft engine nacelles are shown by means of a unique acceleration controlled experiment.

Carl E. Rucker
Aerospace Engineer
NASA Langley Research Center
Langley Station, Hampton, Va.

ABSTRACT

The National Aeronautics and Space Administration is presently sponsoring research which incorporates new materials into the design of jet engine nacelles to reduce the flyover perceived noise levels for commercial air transports. New materials of fibrous composition are being utilized in efforts to reduce jet aircraft noise which adversely affects communities adjacent to commercial airports.

Fatigue data for one class of fibrous material are presented in this paper. The material is composed of random lengths of AISI 347 stainless steel wire, sintered to form a porous structure. This paper contains information on the effects of varying the density, thickness and wire diameter of these materials and the effect of stiffening the wire matrix with supporting screens.

Reversed bending fatigue tests were conducted on constant strength beams at constant tip acceleration and constant stress. Beams were tested at resonance as a cantilevered beam with its base excited by an electromagnetic shaker. The beams were tested to failure or to a minimum of 40 hours and the results are plotted in the form of S-N curves. A progressive change in beam stiffness

with negligible change in beam damping is illustrated from acceleration and strain measurements. Increased fatigue strength is associated with increased density, increased thickness, decreased wire diameter, and with the addition of stiffening wire support screens.

SYMBOLS

E_t $\frac{dS}{d\epsilon}$ = tensile modulus of elasticity, lb/in^2

f_o resonant frequency of beam system, Hz

g acceleration due to gravity, 386 $in./sec^2$

h thickness of beam, in.

L length of beam, in.

N number of fatigue cycles to failure

S axial or bending stress calculated from acceleration or load measurements, lb/in^2

dS incremental change in stress, lb/in^2

t_u tensile ultimate stress, lb/in^2

t_y tensile yield stress, lb/in^2

Δ deflection of beam, in.

ϵ axial or bending strain

$d\epsilon$ incremental change in strain

ρ_p density of AISI 347 stainless steel, lb/in^3

INTRODUCTION

Langley Research Center has been supporting contracts with McDonnell-Douglas Corporation and the Boeing Company for acoustic treatment of turbofan engine nacelles of a type in use on many current commercial jet aircraft[1]. The

main objective of this work is the reduction of flyover noise during landing approach operations. The sources of noise radiated from a turbofan engine are indicated schematically in fig. 1. The noise generated inside the engine radiates primarily from the inlet and the fan discharge ducts, whereas jet noise radiates mainly from the mixing region of the primary jet exhaust. The objective of the application of acoustical duct treatment to the nacelle is the reduction of noise radiated from both the inlet and fan discharge ducts, particularly the high frequency noises associated with the fan.

The manner in which acoustic treatment may be applied to a current turbofan engine is shown in the cut-away sketch of fig. 2. This figure was taken from ref. 2 and shows the treated area of a McDonnell-Douglas nacelle for a DC-8 airplane. It can be seen that treatment has been applied to the inlet and center body surfaces plus an additional concentric splitter ring in the inlet. The fan discharge ducts have been treated over their entire surfaces. Although the performance of such acoustic treatments has not been completely evaluated, the expected results from their use are suggested by the estimates of fig. 3.

Shown in fig. 3 are the noise spectra for both a modified and an unmodified airplane for the condition of landing power and for an observer position approximately 1 mile from touchdown. It can be seen that sharp peaks occur in the spectrum for the unmodified airplane at frequencies above 2 000 Hz, and these peaks are associated with the fan of the engine. The dashed curve is an estimation of the noise spectrum for comparable flight conditions for an aircraft which has been modified by the inclusion of acoustic treatment such as was illustrated in fig. 2. Of particular significance is the marked reduction in amplitude of the discrete frequencies associated with the fan. Although several different materials are under consideration for applications, such as

those of fig. 2, one class of this material has a randomly interlocked structure of metallic fibers as shown by the photographs of fig. 4 and others have a woven filament structure[3].

The purpose of the tests described in this paper is to furnish data for AISI 347 stainless steel fibermetal (see fig. 4) as a basis for initial designs utilizing these materials. Coupons were tested to establish the experimental modulus of elasticity (tensile), the tensile ultimate stress, and tensile yield stress. Reversed bending fatigue life tests were run for nine different material configurations. Fatigue lives were studied by varying the parameters of density, thickness, fiber diameter, and surface reinforcement in "standard" fatigue tests to determine the effects of variation of these parameters[4].

EXPERIMENTAL PROCEDURES

Test Specimen Configurations

The specimens in this test were fabricated from commercially available AISI 347 stainless steel fibermetal panels. The parent material is composed of a maximum of 0.08 percent carbon, 2.00 percent manganese, 0.045 percent phosphorus, 0.030 percent sulphur, 1.00 percent silicon, and also has 17 to 19 percent chromium, 9 to 13 percent nickel, columbium plus tantalum at least 10 times the carbon content, plus the balance in iron. The density of the parent material is 0.29 pounds per cubic inch, the tensile modulus of elasticity is 28.0×10^6 pounds per square inch, the tensile ultimate load is 9.0×10^4 psi (bar anealed), and the endurance limit is 3.9×10^4 psi (anealed)[5]. AISI 347 is an austenitic type (nonhardenable) stainless steel.

The fibers were tooled to random lengths from 0.0018, 0.0028, or 0.0038-inch-diameter wire depending on configuration and were bonded together

in panel configurations by heating in a reducing atmosphere (sintered), and were formed to the correct volume (thickness) and density. The densities of the materials tested were 40 percent, 55 percent, or 70 percent of the density of an equal volume of the parent material. The thicknesses of the materials tested were 0.030, 0.060, or 0.090 inch. Two configurations were reinforced with 18 mesh (18 wires per inch) by 0.009-inch-diameter wire screens or 30 mesh (30 wires per inch) by 0.0075-inch-diameter wire screens on both surfaces. Screens were fabricated with regular "window screen" rectangular grids from AISI 347 stainless steel and were sintered to both surfaces of the random wire material.

Sixteen tensile coupons and forty-four fatigue coupons were cut from four 12.5 inches by 16 inches commercially available fibermetal panels of each configuration. Each of the panels were cut into 11 fatigue coupons and 4 tensile coupons (fig. 5). Electro discharge machining technique resulted in excellent edge conditions, with wires left relatively undisturbed adjacent to the cut. Fatigue coupons were selected in a random manner to prevent biasing of data due to sheet selection and location in the sheet. All tensile specimens were tested for each configuration of fibermetal, whereas only a portion of the fatigue coupons were tested.

Tensile Tests

Standard tensile tests were run using a conventional hydraulic load machine. A one-inch gage length extensometer was used to measure strain. Load versus strain was recorded on an x-y plotter.

Load-strain curves were obtained from tensile tests and E_t, t_u, and t_y were determined using techniques outlined in Mil Handbook 5A[6]. (See for example

fig. 6.) A stress-strain curve based on measured specimen areas and load-strain curves, is used to determine E_t which is defined as the slope of the straight line portion of the curve. T_y is computed from the intersection of the stress-strain curve and a line having the slope E_t and intersecting the abscissa at the value 0.001 inch per inch. T_u is the ultimate load divided by the specimen area.

Fatigue Tests

Most of the fatigue testing was accomplished on a 300-pound force electromagnetic shaker system (fig. 7). The materials tested for obtaining the effects of density were begun on 50-pound force shakers, where some difficulties were encountered in loading the stronger materials.

The specimens were mounted as cantilever beams as shown in the fig. 7. An oscillator capable of adjusting the frequency to an accuracy of 0.01 Hz was used to set the driving frequency and amplitude of vibration.

At the beginning of each test the driving frequency was varied at a relatively small amplitude in order to determine the approximate first natural bending vibration mode of the specimen. The fatigue tests were then accomplished at the beam natural frequency at various root stress levels.

The stress levels were determined with the aid of a piezo-resistive or piezo-electric accelerometer on the free end of the beam. The specimens were tested over a range of accelerations. Acceleration measurements were accurate within ±3 percent for the 1 gram, 3 m.v./g piezo-resistive accelerometer which was used during most of the testing for evaluating change of the density parameter. Acceleration measurements were accurate within ±1 percent for the 3 gram, 5.5 m.v./g piezo-electric accelerometer which was used during the

balance of testing and for all tests for which the peak acceleration at the tip exceeded ±150g.

The specimens were tuned to resonance (f_o) by monitoring the tip accelerometer at very low loads. The peak deflection Δ and the peak acceleration g are then related by the following formula

$$g = 0.102\ f^2\ \Delta \tag{1}$$

The beam was assumed to be a constant strength beam whose stress S is related to the deflection by[7]:

$$\Delta = \frac{SL^2}{E_t h} \tag{2}$$

For these studies the thicknesses, h, were 0.030, 0.060, and 0.090 inch. The length of the beam L was 4.3 inches and E_t was determined for each configuration by averaging the results from 16 tensile tests.

Supplementary instrumentation included a strain gage at the root of the beam and a reference piezo-electric accelerometer located on the base-clamp which held the test specimen. The strain gages were axial, advanced alloy, epoxy backed gages of 3/16 inch gage length rated for aluminum. The overall gage length including tabs was 0.26 inch and the grid width was 0.1 inch. The gages were installed by impregnating a 0.0005 inch thickness long fiber glass felt with gage mounting cement and laying the glass felt on the fibermetal surface where the gage was to be installed. The felt prevented "wicking" of the cement into the fibermetal pores and furnished a durable mounting.

Test data were monitored by root-mean-square voltage to dc converters (voltmeters). The output strain and output tip acceleration analog signals were monitored on a strip chart recorder. The input frequency was measured from the oscillator on a frequency counter, and the number of cycles accumulated

were measured from the tip accelerometer by a counter in the continuous counting mode.

A sample strip chart recording is shown in fig. 8. At the start of the test, acceleration was increased quickly to the desired level and was held essentially constant (typical variation was ±0.5 "g" rms) for the duration of the test. As the test progressed, the natural frequency of the model decreased, probably because of reorientation of fibers, fracture of fiber bonds, breaking of the fibers, or some combination of these phenomena. The driving frequency was thus periodically readjusted to the new resonance values. Frequent adjustments of the input frequency and the tip acceleration as the beam stiffness decreased, resulted in essentially a constant loading force and constant root strain as seen from the acceleration and strain records of fig. 8.

RESULTS AND DISCUSSION

Tensile Tests

Values of E_t, T_y, and T_u were determined for each of the tensile specimens according to the methods of ref. 5 as illustrated in fig. 6. The average values for these data for each of the nine configurations are given in Table 1. It can be seen from the table that increases in density and thickness of specimens, a decrease in the fiber diameter, and the addition of surface reinforcement screens had the effect of improving the mechanical properties of these materials.

Fatigue Tests

A sufficient number of specimens was tested to failure for the combinations of parameters of fig. 9, to allow the definition of S-N curves of the type shown

in figs. 10 to 13, where each data point represents a single test failure. In each case the curves are faired through the data points as an aid in the interpretation of the data. As an example, the data of fig. 10 illustrate the effects of model thickness for a constant fiber diameter and material density. It can be seen that at a given stress level the greater number of cycles to failure is associated with the greater model thickness. Following the same manner of presentation, the data of figs. 11, 12, and 13 indicate that a greater number of cycles to failure is associated, respectively, with an increase in material density, a decrease in fiber diameter and the addition of surface reinforcement screens.

The quantity S, which is the calculated stress based on acceleration measurements, and the quantity N, the number of cycles to failure are plotted in figs. 10 to 13 and are tabulated in Table 2. Also included in Table 2 are measured resonant frequencies f_o, measured peak accelerations g, calculated peak deflections Δ, and stresses $E\epsilon$ based on measurements of axial strains ϵ and E_t from Table 1.

The endurance limit, which is the limiting value of the stress below which the material can presumably endure an infinite number of stress cycles (where the S-N curve becomes horizontal), can be determined from the figures. As an example, an endurance limit of 4800 psi is estimated from 11 tests of the 0.030 inch thickness material from the lower curve of fig. 10.

CONCLUDING REMARKS

Reversed bending fatigue and tensile tests have been conducted for stainless steel fiber metal material for a range of geometric parameters. The results indicate that increased fatigue life and tensile strength were

associated with increased model thickness, increased material density, decreased fiber diameter and with the addition of surface reinforcement screens.

REFERENCES

1. Progress of NASA Research Relating to Noise Alleviation of Large Subsonic Jet Aircraft. A conference held at the Langley Research Center, Hampton, Virginia, October 8-10, 1968. NASA SP-189.
2. Watson, Herschel A., Jr.: Structural and Enviromental Studies of Duct Lining Acoustical Materials. Presented at the 77th Meeting of the Acoustical Society of America, April 8-10, 1969.
3. Scott, David H.: Fatigue Evaluation of Noise Suppression Materials. Presented at the 76th Meeting of the Acoustical Society of America, Cleveland, Ohio, November 18-22, 1968.
4. Anon.: A Guide for Fatigue Testing and the Statistical Analysis of Fatigue Data. ASTM Special Publication No. 914, (2nd ed.), 1963.
5. Materials in Design Engineering - Materials Selector Issue, vol. 64, no. 5, 83 (Mid-October 1966-67).
6. Anon.: Metallic Materials and Elements for Aerospace Vehicle Structures. Department of Defense MIL-Handbook-5A, February 8, 1968 (Superseded MIL-Handbook-5, August 1962).
7. Miller, F. E.; and Doevinsfeld, H. A.: Mechanics of Materials 2nd ed., International Text Book Co., Scranton, Penn., 10 (1962).

TABLE 1.- AVERAGE VALUES FOR SIXTEEN TENSILE TESTS ON FIBERMETAL MATERIAL

Parameter studied	Percentage, ρ_p	Thickness, h	Fiber diameter	Reinforcement mesh/fiber diameter	E_t, (x 10^{-6}psi)	T_y, (psi)	T_u, (psi)
Density	40	0.060	0.0028	None	1.91	2813	7858
Density	55	.060	.0028	None	3.01	4894	13194
All except reinforcement	70	.060	.0028	None	8.83	12928	26149
Thickness	70	.030	.0028	None	7.14	11333	22264
Thickness	70	.090	.0028	None	9.03	13694	27552
Wire diameter	70	.060	.0018	None	9.86	16062	30633
Wire diameter, reinforcement	70	.060	.0038	None	6.81	10723	21721
Reinforcement	70	.060	.0038	30/0.0075 in.	9.06	10470	23550
Reinforcement	70	.060	.0038	18/0.009 in.	7.70	12032	23835

TABLE 2.- FATIGUE TEST RESULTS FOR 347 STAINLESS STEEL FIBERMETAL BEAMS WITH REVERSED BENDING LOADING

Initial resonant frequency, f_o(Hz)	Zero to peak acceleration, "g"	Zero to peak deflection Δ(in.)	R.M.S. stress from strain gage, Eϵ(ksi)	Zero to peak stress, S(ksi)	Cycles to failure, N(millions)	Remarks
Configuration: 0.030-in.-thickness, 70% ρ_p density, 0.0028-in.-diam fiber; results plotted in figure 10						
23.2	47.1	0.858	9.53	10.00	0.050	
26.6	55.8	.773	9.14	9.00	.019	
25.5	51.2	.773	8.00	9.00	.018	
23.2	37.7	.687	7.43	8.00	.121	
24.0	40.4	.687	7.28	8.00	.167	
25.7	38.2	.567	8.28	6.60	.303	
25.1	33.1	.515	6.85	6.00	.390	
25.7	33.5	.498	5.71	5.80	.506	
26.6	31.0	.427	6.00	5.00	4.436	
26.3	29.7	.421	5.64	4.90	3.628	
26.3	29.1	.412	5.86	4.80	6.502	No failure
25.9	31.7	.464	5.43	5.40	2.353	
Configuration: 0.090-in.-thickness, 70% ρ_p density, 0.0028-in.-diam fiber; results plotted in figure 10						
91.5	194.2	0.228	7.41	10.00	0.237	
91.5	213.7	.250	10.29	11.00	.132	
81.0	193.2	.292	11.74	12.84	.038	
90.1	161.0	.195	7.04	8.55	.997	
99.1	182.2	.182	7.51	8.00	.967	
82.6	121.8	.175	5.78	7.70	6.751	No failure
88.7	142.4	.177	6.68	7.80	5.479	
99.2	182.6	.182	6.50	8.00	2.450	
87.8	164.5	.209	8.49	9.20	.793	
Configuration: 0.060-in.-thickness, 70% ρ_p density, 0.0028-in.-diam fiber; results plotted in figs. 10,11,&12						
57	83	0.251	-----	7.55	6.800	No failure
55	134	.434	10.67	13.01	.029	
55	125	.405	10.14	12.14	.092	
61	143	.376	8.36	11.27	.081	
55.5	119	.379	10.32	11.36	.208	
59	119	.335	10.32	10.04	.087	
52.5	93	.331	6.76	9.92	.563	
60.5	109	.292	-----	8.75	2.199	
57	106	.323	8.71	9.68	.176	
56	98	.306	7.83	9.17	.625	
60	110	.300	7.47	8.99	.529	
57.5	98	.291	7.65	8.72	.492	
55.5	91.7	.292	7.83	8.75	.906	
61	110.7	.288	6.94	8.63	.865	
58.5	94.7	.272	8.45	8.15	.782	
59.9	99.0	.271	6.85	8.12	1.665	
56.8	84.8	.278	5.96	7.63	4.620	No failure
Configuration: 40% ρ_p density, 0.060-in.-thickness, 0.0028-in.-diam fiber; results plotted in figure 11						
45	72 (est)	0.349	2.75	2.16	0.0087	Accelerometer failed
35	95.0	.760	2.79	4.70	.0020	
43	77.0	.408	2.53	2.53	.0122	
34	38.0	.322	1.69	1.99	.1221	
39	63.0	.406	1.43	2.51	.0140	
38	56.7	.385	2.17	2.38	.0165	
35	49.7	.397	1.84	2.46	.1056	
38	59.1	.401	2.13	2.48	.0250	
40	58 (est)	.355	2.09	2.20	.0184	Accelerometer failed
33.5	70.6	.617	3.08	3.82	.0018	
37.5	72.8	.508	2.42	3.14	.0036	
38	42.0	.285	1.47	1.76	.0881	
38	35.0	.238	1.32	1.47	1.6412	No failure
38	35.0	.238	1.58	1.47	1.8652	No failure
34	31.0	.263	1.69	1.63	.3156	
Configuration: 55% ρ_p density, 0.060-in.-thickness, 0.0028-in.-diam fiber; results plotted in figure 11						
50	101.0	0.396	3.30	3.87	0.073	
53	113.4	.396	3.47	3.87	.037	
43.5	114.8	.600	6.66	5.86	.003	
50	113.4	.445	3.19	4.34	.021	

TABLE 2.- FATIGUE TEST RESULTS FOR 347 STAINLESS STEEL FIBERMETAL BEAMS WITH REVERSED BENDING LOADING - Concluded

Initial resonant frequency, f_o(Hz)	Zero to peak acceleration, "g"	Zero to peak deflection Δ(in.)	R.M.S. stress from strain gage, Eϵ(ksi)	Zero to peak stress, S(ksi)	Cycles to failure, N(millions)	Remarks
Configuration: 55% ρ_p density, 0.060-in.-thickness, 0.0028-in.-diam fiber; results plotted in figure 11 - continued						
55	69.2	0.224	2.55	2.19	2.751	No failure
65	128.0	.297	2.49	2.90	.186	
49	72.0	.295	1.91	2.88	.789	
56	84.0	.262	2.20	2.59	1.578	No failure
45.5	80.0	.379	2.66	3.70	.067	
Configuration: 0.0018-in.-diam fiber, 70% ρ_p density, 0.060-in.-thickness; results plotted in figure 12						
61.0	156.6	0.413	11.64	13.20	0.061	
60.0	137.7	.375	10.37	12.00	.182	
59.8	116.0	.317	8.18	10.17	1.109	
61.2	109.9	.288	7.69	9.20	1.380	
63.2	114.6	.281	7.69	9.00	1.101	
65.0	121.2	.281	8.28	9.00	1.536	
64.5	116.7	.275	7.69	8.80	.738	
62.1	106.5	.269	8.48	8.60	2.373	
61.3	96.6	.252	7.89	8.07	4.114	
64.0	108.5	.260	7.10	8.33	2.829	
64.3	105.4	.250	7.40	8.00	6.939	No failure
Configuration: 0.0038-in.-diam fiber, 70% ρ_p density, 0.060-in.-thickness; results plotted in figs.12 & 13						
55.2	75.96	0.244	4.35	5.40	7.800	No failure
69.5	133.8	.272	5.64	6.00	.433	
66.7	119.1	.262	5.71	5.80	1.634	
55.6	91.3	.290	5.98	6.40	.687	
60.7	-----	-----	5.98	-----	.546	Accelerometer failed-no plot
51.5	71.4	.264	5.45	5.83	1.693	
52.5	89.05	.317	6.39	7.00	.280	
51.5	122.4	.453	6.73	10.00	.043	
51.9	99.63	.362	6.32	8.00	.181	
50.5	------	-----	6.67	-----	.215	Cable failed - no plot
48.4	60.56	.253	4.22	5.60	4.613	No failure
Configuration: 18 mesh screens, 0.0038-in.-diam fiber, 70% ρ_p density, 0.060-in.-thickness; results plotted in figure 13						
54.0	100.13	0.336	6.48	8.50	0.165	
53.0	94.24	.349	6.78	8.82	.154	
56.0	135.90	.424	7.39	10.73	.057	
54.6	90.32	.297	6.48	7.50	.381	
50.6	72.41	.277	5.24	7.00	.514	
48.6	64.41	.267	5.16	6.75	3.220	
54.4	89.43	.296	5.39	7.48	.490	
57.4	86.49	.257	4.62	6.50	1.113	
49.4	61.61	.247	4.66	6.25	2.521	
48.9	57.96	.237	4.85	6.00	9.767	No failure
58.0	83.24	.242	4.93	6.13	1.569	
52.3	67.68	.242	5.08	6.13	1.413	
54.6	72.24	.237	4.62	6.00	2.324	
49.5	59.38	.237	4.62	6.00	9.064	No failure
Configuration: 30 mesh screens, 0.0038-in.-diam fiber, 70% ρ_p density, 0.060-in.-thickness; results plotted in figure 13						
49.3	72.51	0.292	7.07	8.60	0.295	
54.7	83.06	.272	7.43	8.00	.683	
50.7	64.65	.247	5.80	7.25	8.845	No failure
51.3	68.50	.255	5.80	7.50	2.551	
53.7	77.58	.264	6.70	7.75	2.041	
49.7	68.57	.272	7.43	8.00	.668	
47.4	60.43	.264	7.25	7.75	6.701	No failure
51.4	74.40	.268	7.07	7.88	.561	
54.0	78.42	.264	6.16	7.75	3.310	
57.9	87.23	.255	6.70	7.50	1.173	
54.2	76.43	.255	6.10	7.50	1.172	
53.2	73.65	.255	6.01	7.50	1.537	
48.9	61.19	.251	6.01	7.38	9.600	No failure
47.6	78.62	.340	7.97	10.00	.155	

CAPTIONS

Figure 1.- Illustration of sources of noise emitted by turbofan engines

Figure 2.- Cutaway view of modified turbofan engine nacelle showing treatment of inlet and fan ducts with acoustic material

Figure 3.- Estimated flyover noise spectra for modified and unmodified four engine fan jet aircraft at time of peak instantaneous perceived noise level at an altitude of 370 feet using landing power

Figure 4.- Illustration of random wire felt fibermetal construction showing screen reinforcement and typical cross-section

Figure 5.- Drawings of tensile test and fatigue test models

Figure 6.- Sample stress-strain curve for fibermetal tensile test showing manner of determination of elastic properties

Figure 7.- Test set-up showing fibermetal fatigue coupon mounted as a cantilever beam on a 300 pound force shaker

Figure 8.- Samples of time averaged values of the peak acceleration and strain response time histories for a fibermetal beam fatigue test

Figure 9.- Summary listing of test parameters showing test constants and ranges of variables

Figure 10.- The effects of model thickness on the reversed bending fatigue behavior of 70 percent ρ_p density, 0.0028-inch-fiber diameter 347 stainless steel fibermetal beams

Figure 11.- The effects of model density on the reversed bending fatigue behavior of 0.060-inch-thickness, 0.0028-inch-fiber diameter 347 stainless steel fibermetal beams

Figure 12.- The effects of model fiber diameter on the reversed bending fatigue behavior of 0.060-inch-thickness, 70 percent ρ_p density 347 stainless steel fibermetal beams

Figure 13.- The effects of model surface screen reinforcement on the reversed bending fatigue behavior of 0.060-inch-thickness, 70 percent ρ_p density, 0.0038-inch-fiber diameter 347 stainless steel fiber metal beams

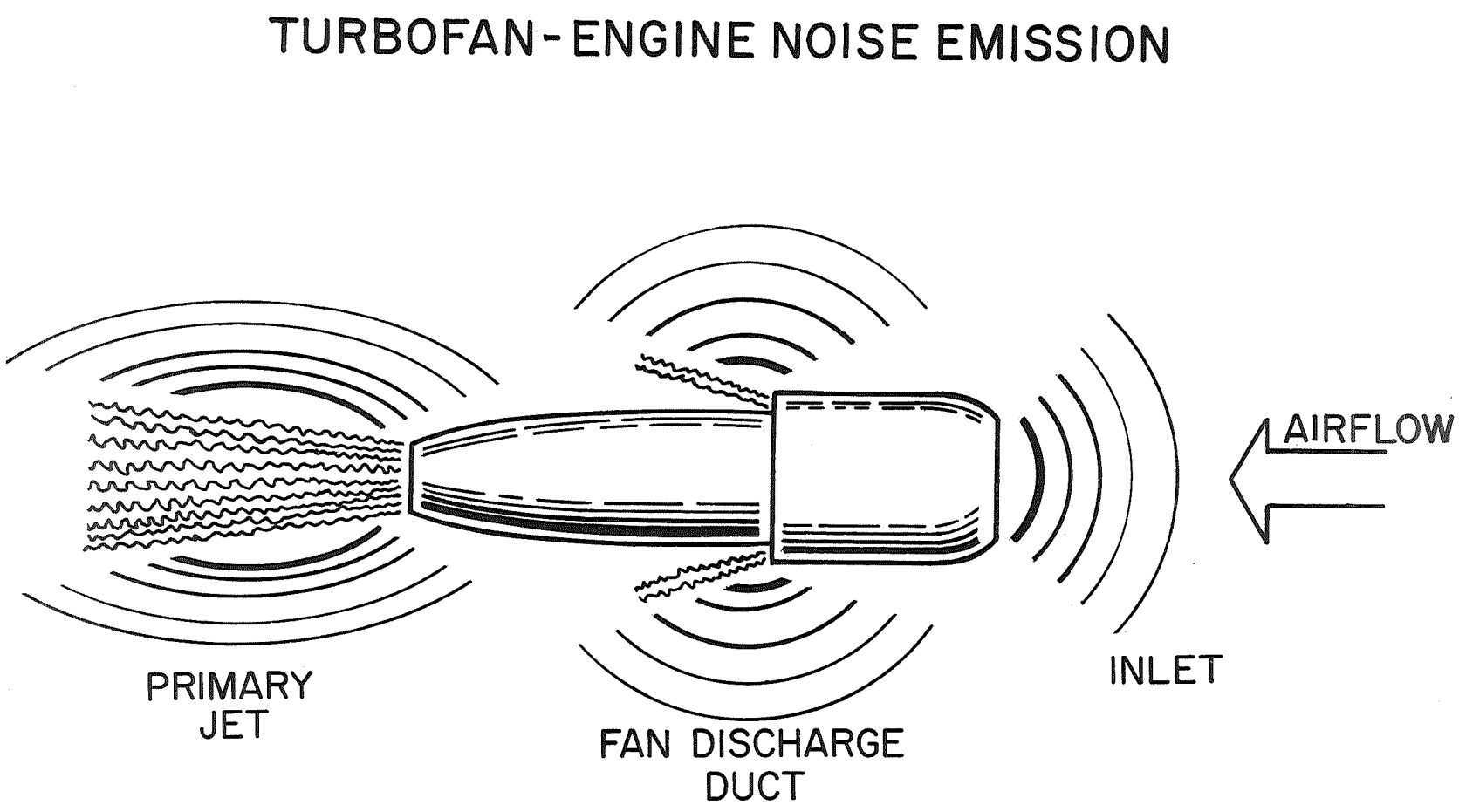

Figure 1.- Illustration of sources of noise emitted by turbofan engines.

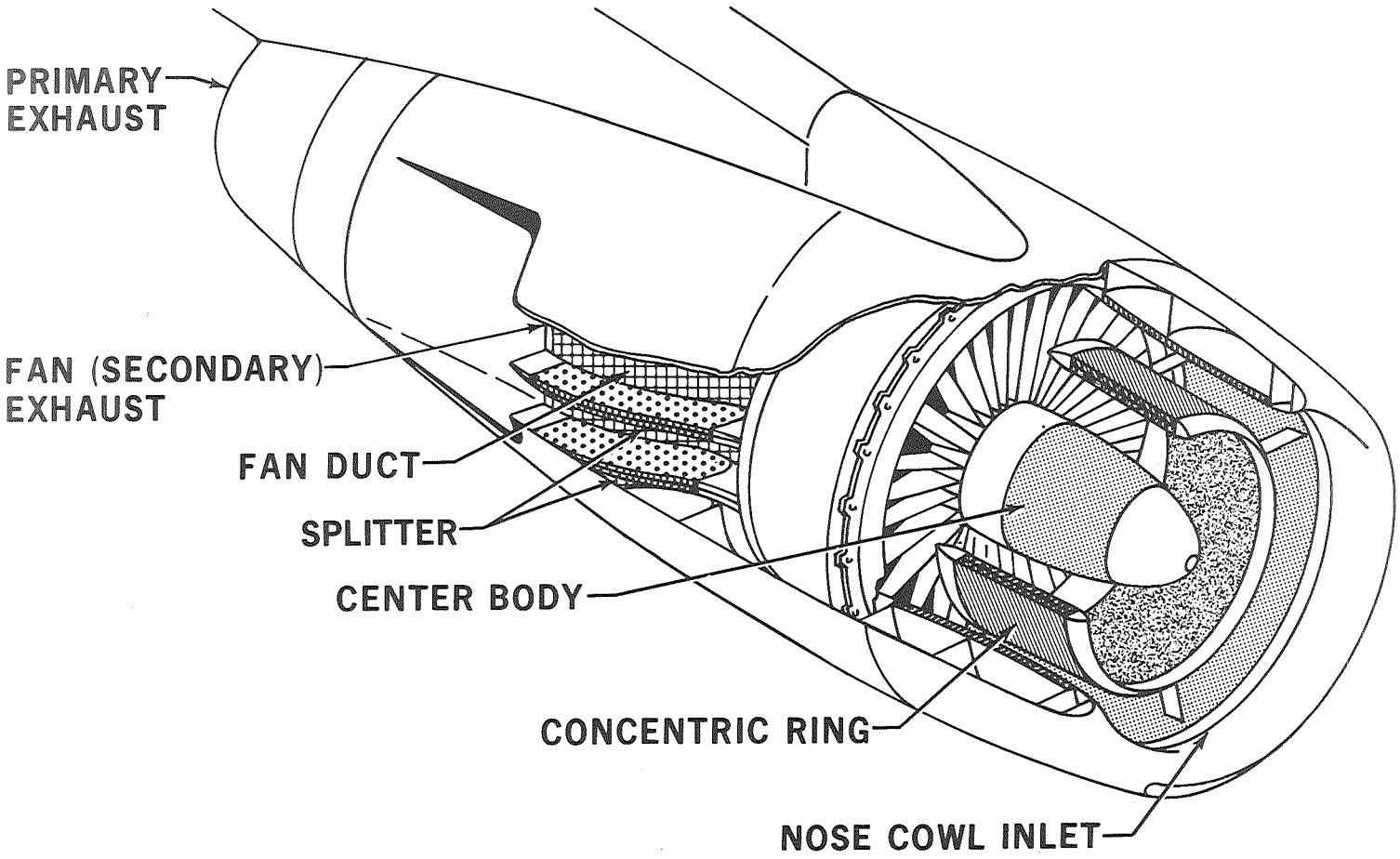

Figure 2.- Cutaway view of modified turbofan engine nacelle showing treatment of inlet and fan ducts with acoustic material.

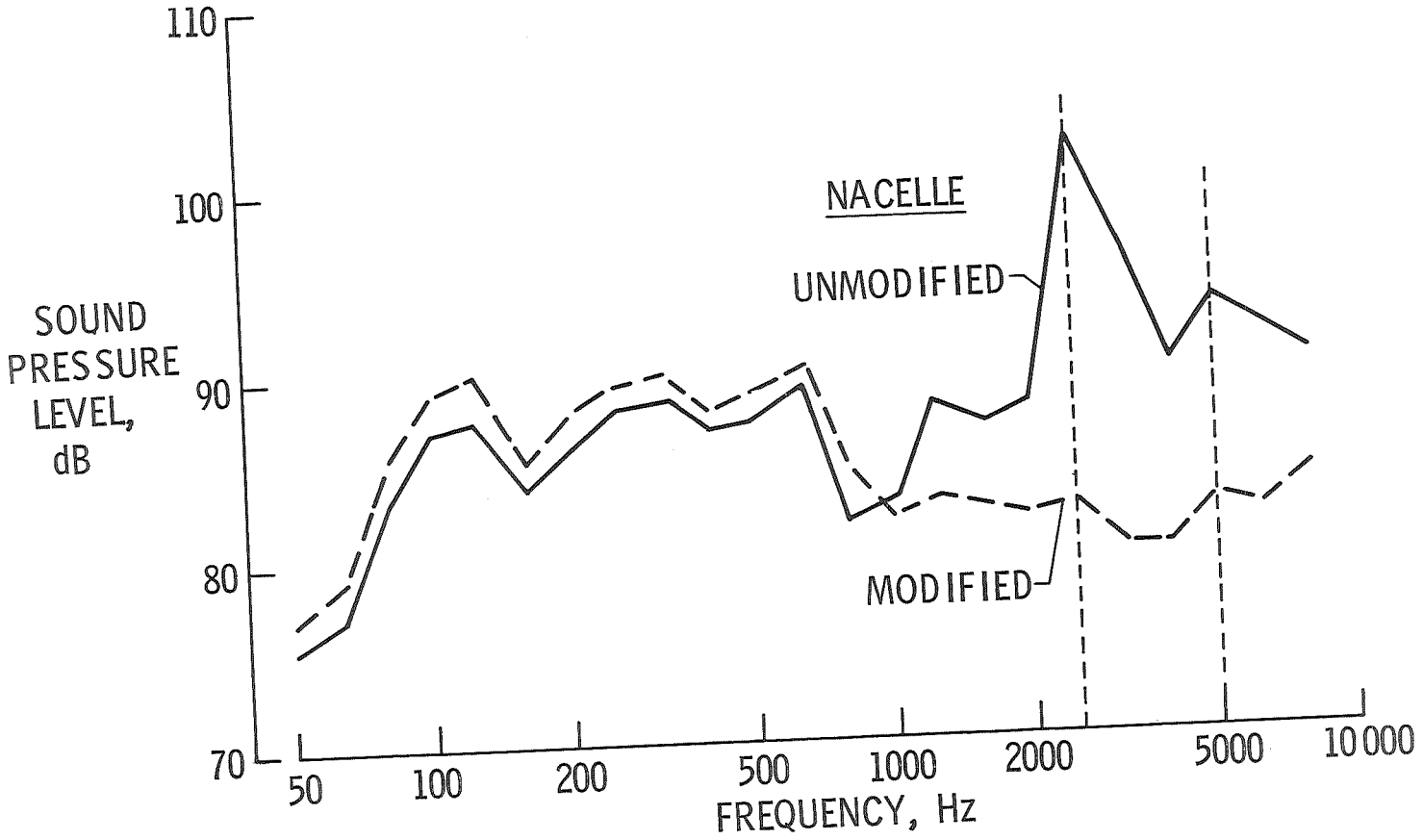

Figure 3.- Estimated flyover noise spectra for modified and unmodified four engine fan jet aircraft at time of peak instantaneous perceived noise level at an altitude of 370 feet using landing power.

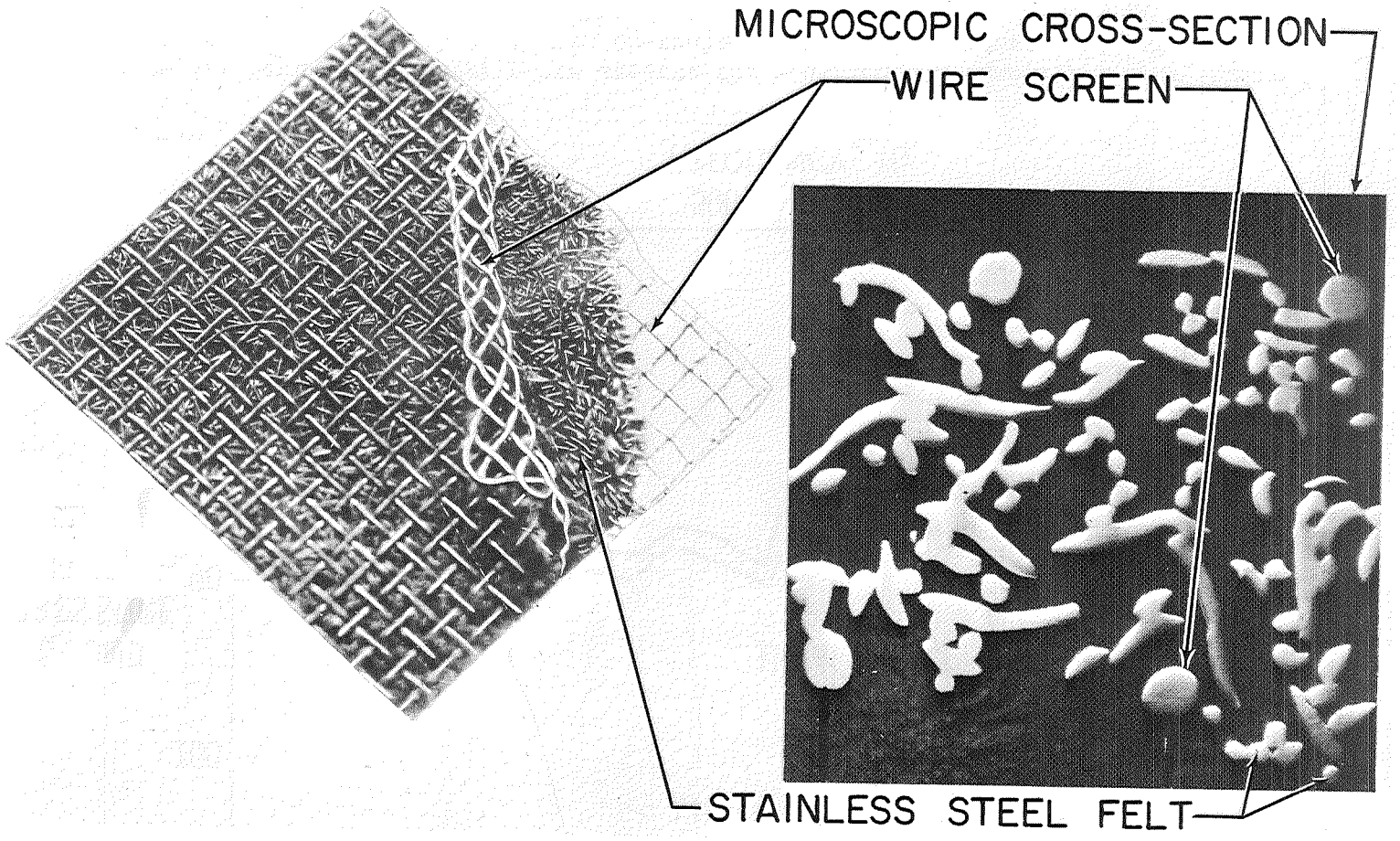

Figure 4.- Illustration of random wire felt fibermetal construction showing screen reinforcement and typical cross section.

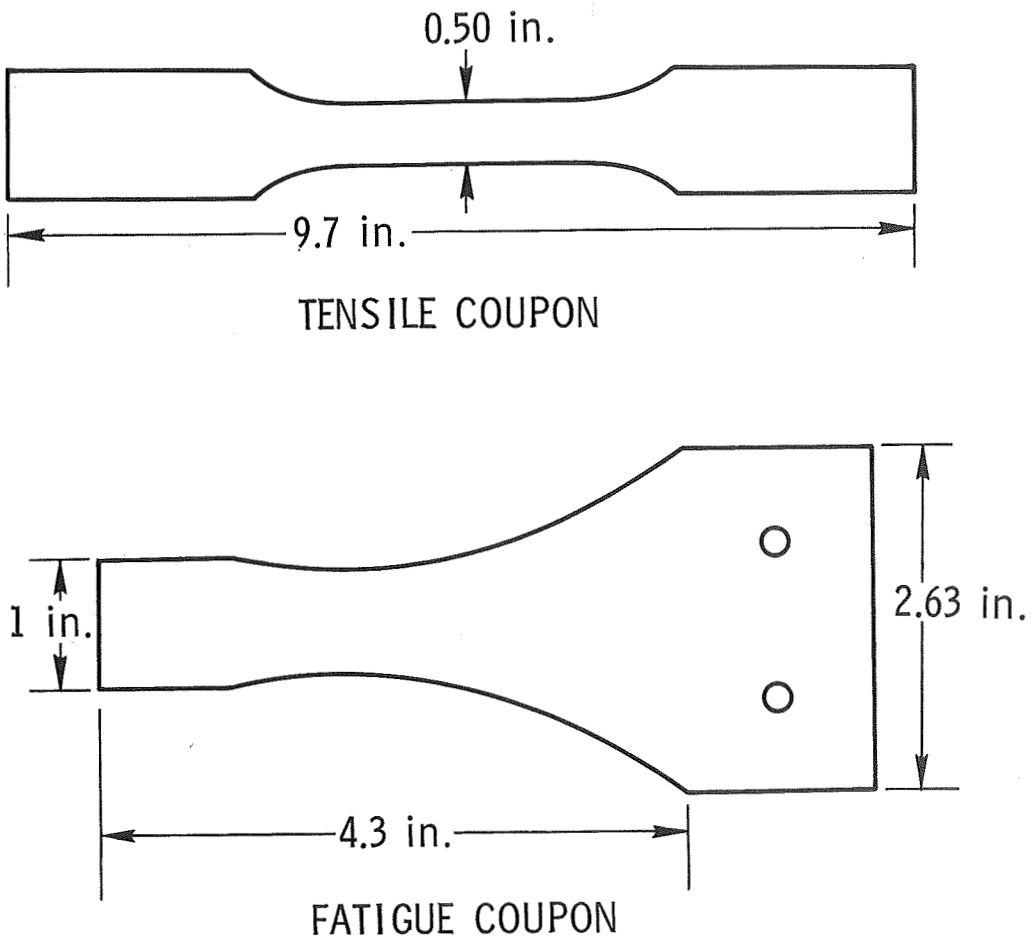

Figure 5.- Drawings of tensile test and fatigue test models.

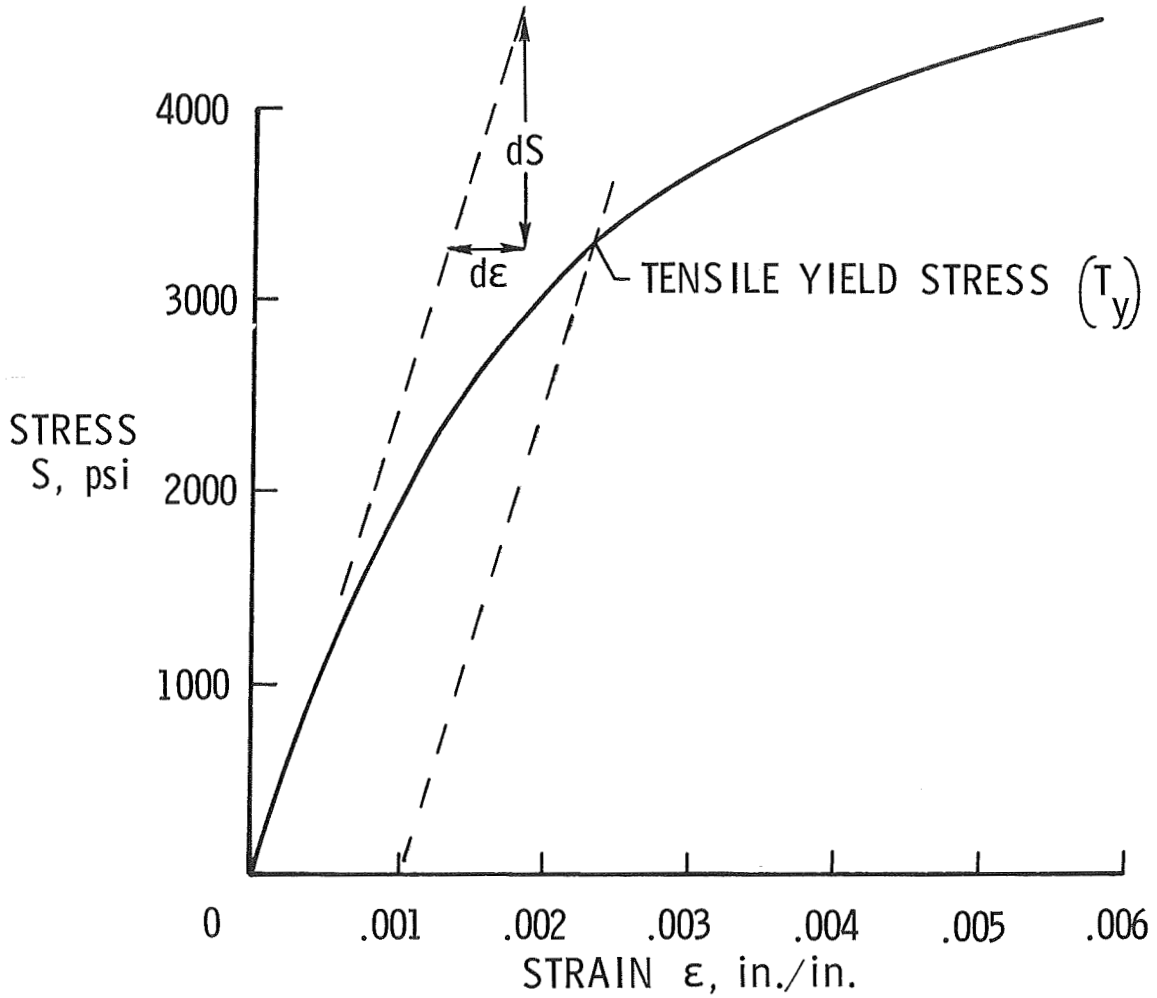

Figure 6.- Sample stress-strain curve for fibermetal tensile test showing manner of determination of elastic properties.

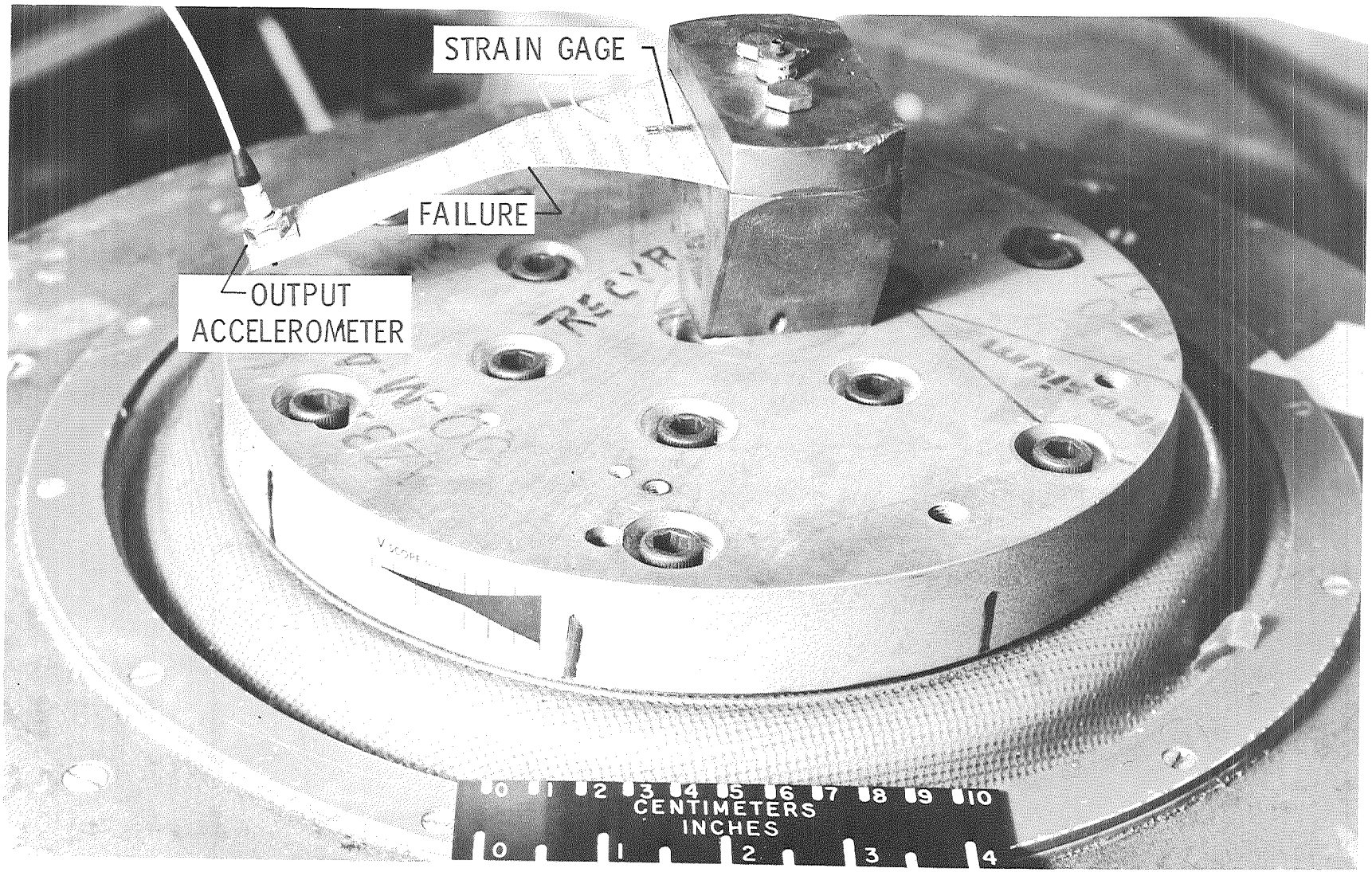

Figure 7.- Test setup showing fibermetal fatigue coupon mounted as a cantilever beam on a 300-pound force shaker.

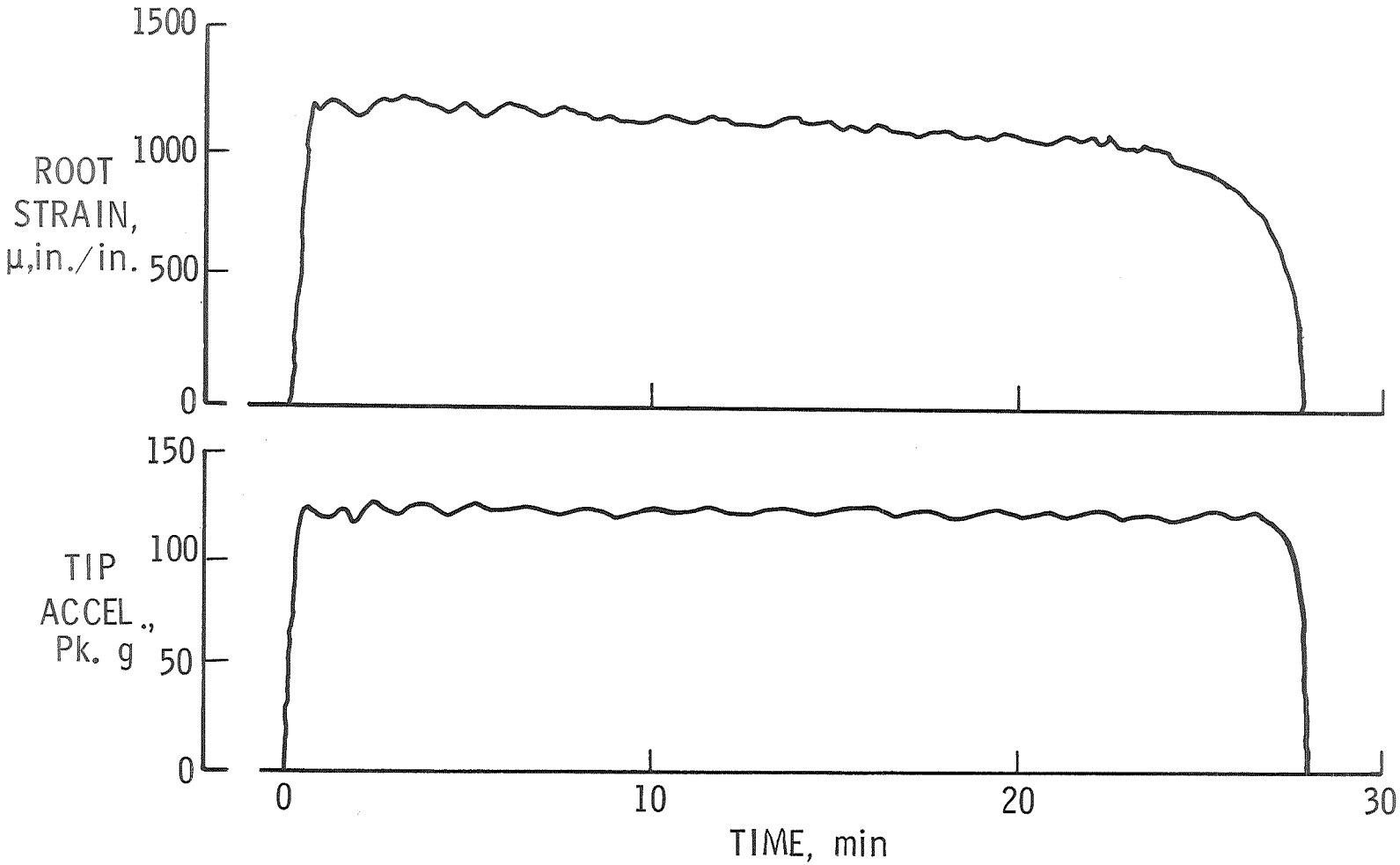

Figure 8.- Samples of time averaged values of the peak acceleration and strain response time histories for a fibermetal beam fatigue test.

VARIABLE	RANGE OF VARIABLE	FACTORS HELD CONSTANT
THICKNESS	0.030", .060", .090"	FIBER DIAMETER, DENSITY
FIBER DIAMETER	0.0018", .0028", .0038"	DENSITY, THICKNESS
DENSITY	40 PERCENT, 55 PERCENT, 70 PERCENT	FIBER DIAMETER, THICKNESS
SURFACE SCREENS	NONE, 18 MESH, 30 MESH	FIBER DIAMETER, THICKNESS, DENSITY

Figure 9.- Summary listing of test parameters showing test constants and ranges of variables.

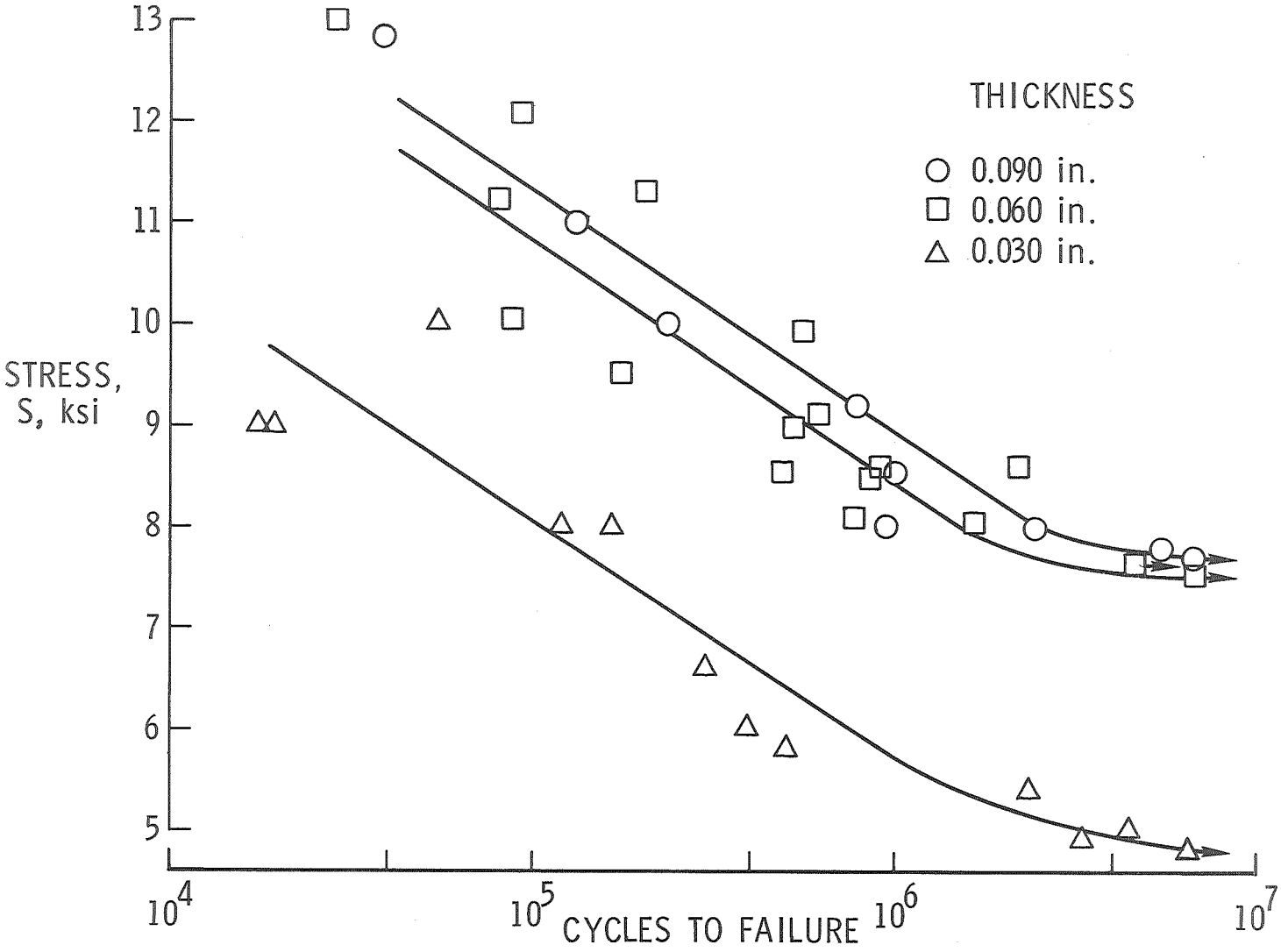

Figure 10.- The effects of model thickness on the reversed bending fatigue behavior of 70 percent ρ_p density, 0.0028-inch fiber diameter 347 stainless steel fibermetal beams.

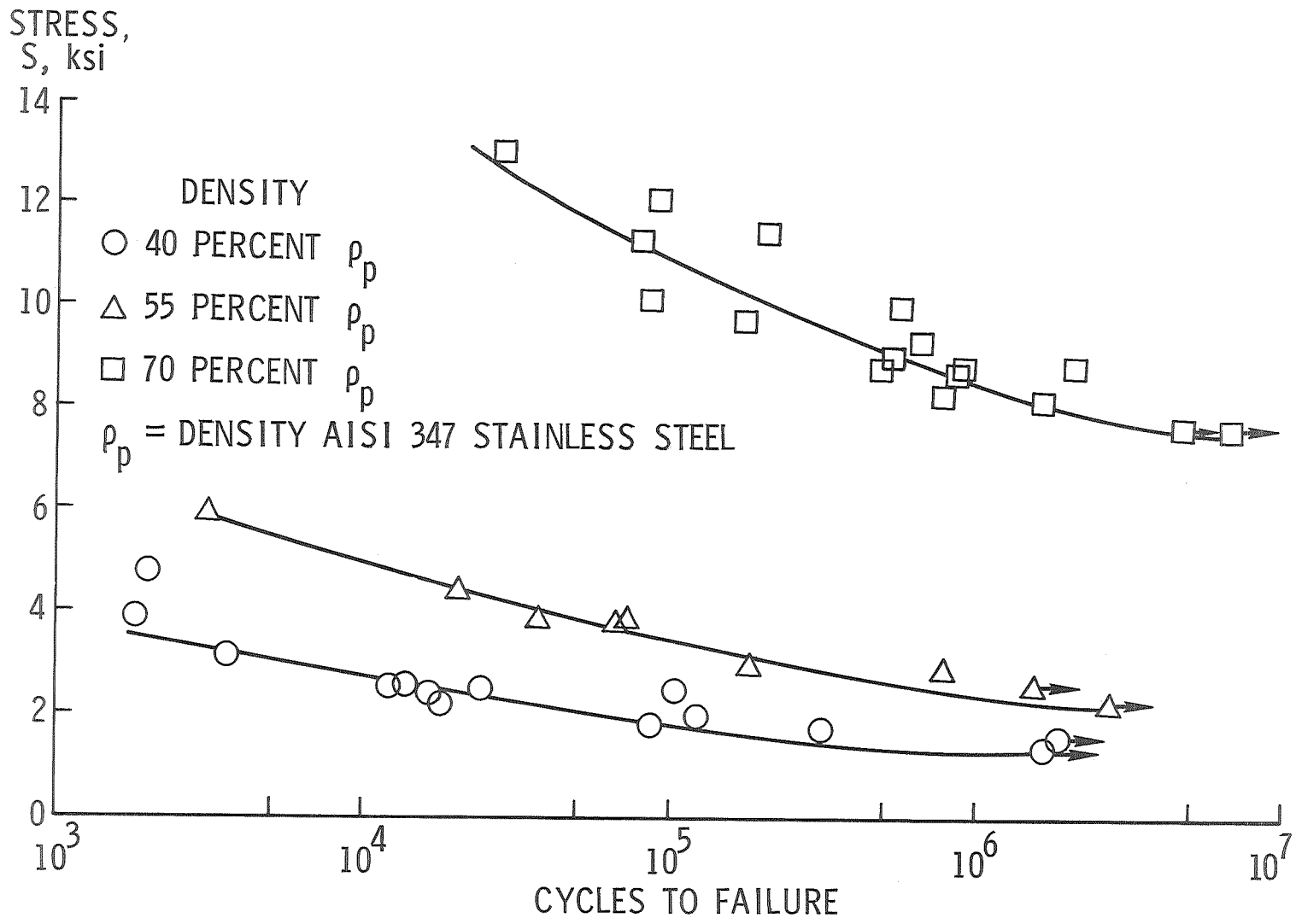

Figure 11.- The effects of model density on the reversed bending fatigue behavior of 0.060-inch thickness, 0.0028-inch fiber diameter 347 stainless steel fibermetal beams.

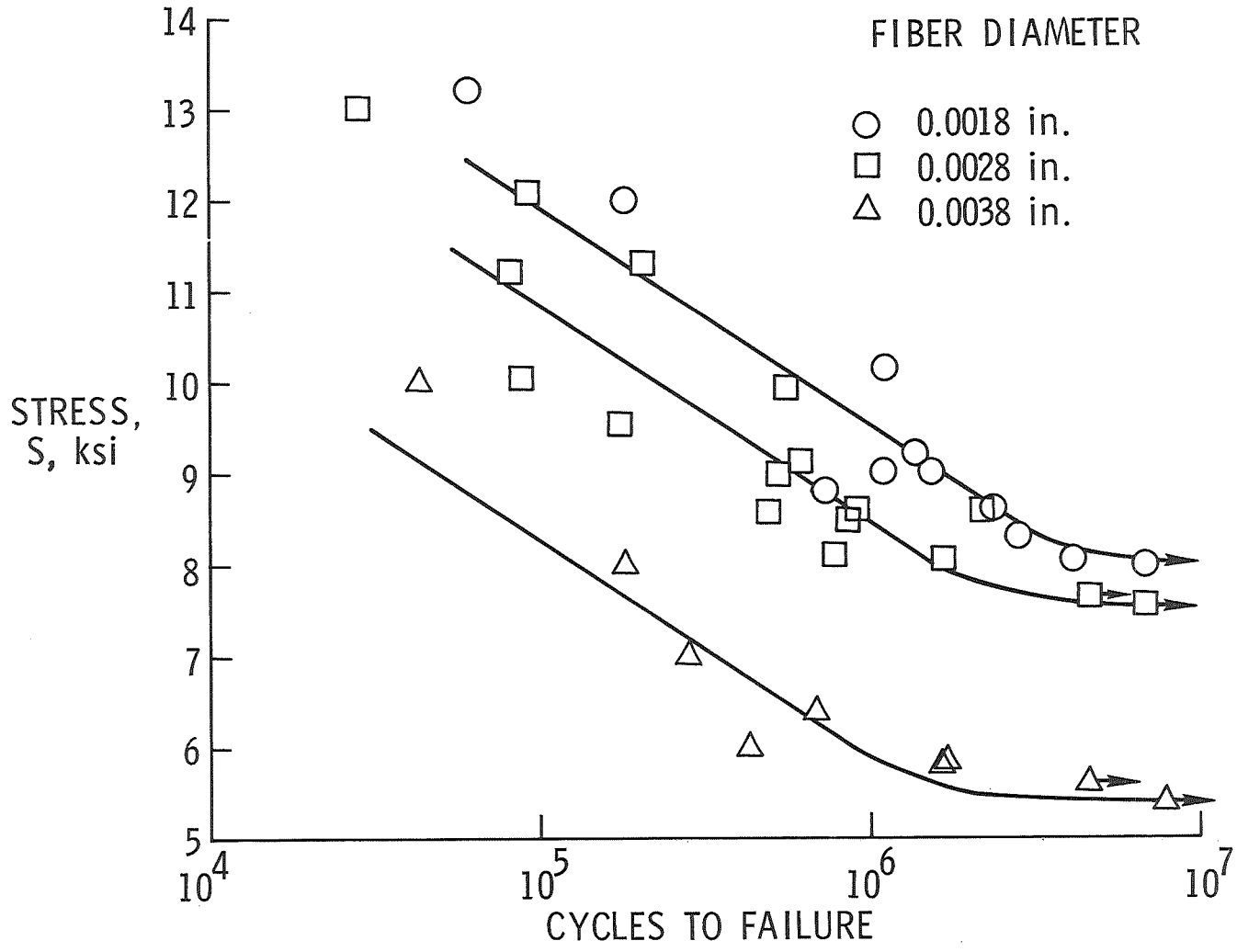

Figure 12.- The effects of model fiber diameter on the reversed bending fatigue behavior of 0.060-inch thickness, 70 percent ρ_p density 347 stainless steel fibermetal beams.

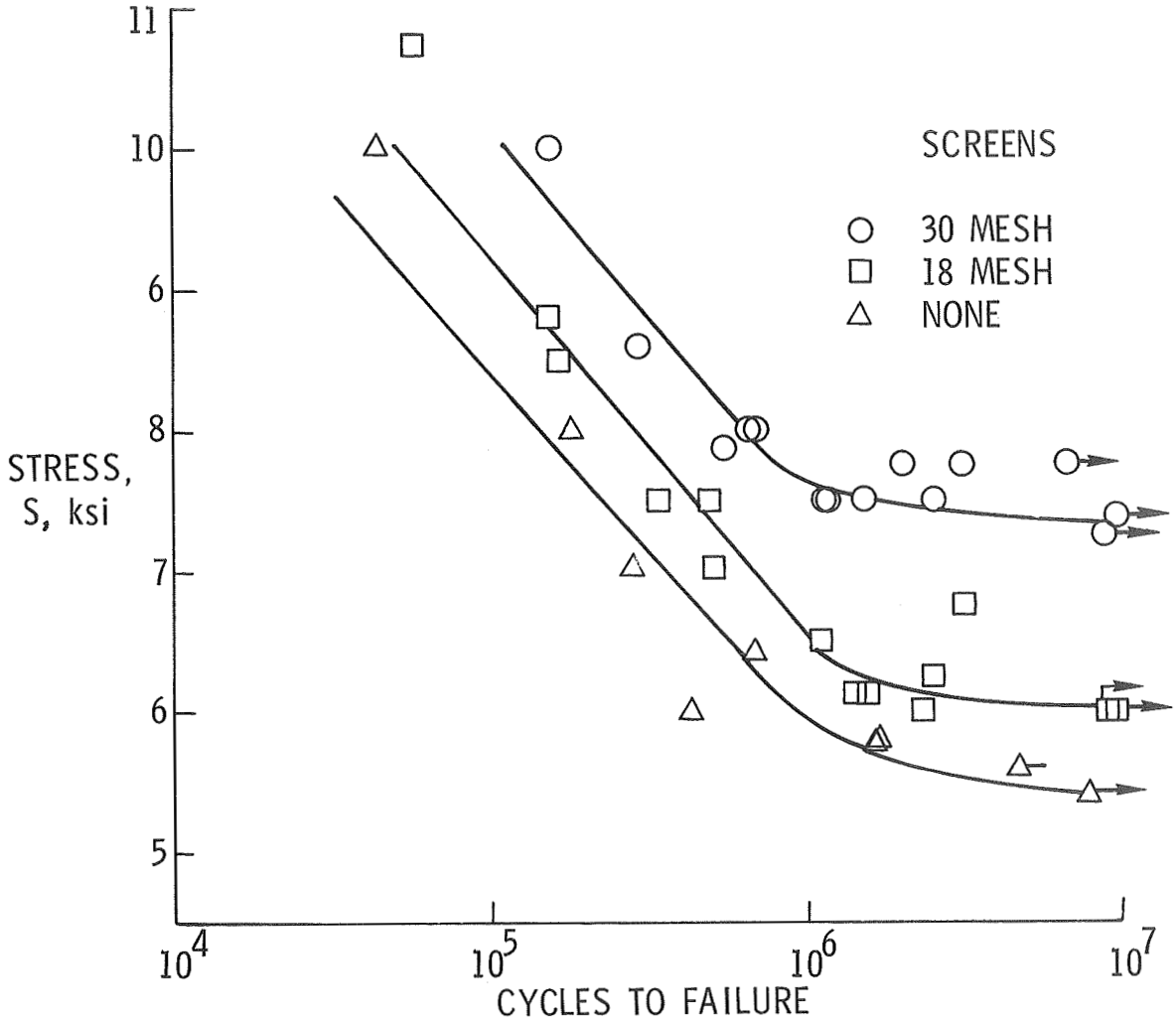

Figure 13.- The effects of model surface screen reinforcement on the reversed bending fatigue behavior of 0.060-inch thickness, 70 percent ρ_p density, 0.0038-inch fiber diameter 347 stainless steel fibermetal beams.

NASA-Langley, 1969